nature immunology

# Mechanistic and structural insight into the functional dichotomy between IL-2 and IL-15

Aaron M Ring[1,2], Jian-Xin Lin[3], Dan Feng[1,2], Suman Mitra[3], Mathias Rickert[1,2], Gregory R Bowman[4], Vijay S Pande[4], Peng Li[3], Ignacio Moraga[1,2], Rosanne Spolski[3], Engin Özkan[1,2], Warren J Leonard[3] & K Christopher Garcia[1,2]

**Interleukin 15 (IL-15) and IL-2 have distinct immunological functions even though both signal through the receptor subunit IL-2Rβ and the common γ-chain ($\gamma_c$). Here we found that in the structure of the IL-15–IL-15Rα–IL-2Rβ–$\gamma_c$ quaternary complex, IL-15 binds to IL-2Rβ and $\gamma_c$ in a heterodimer nearly indistinguishable from that of the IL-2–IL-2Rα–IL-2Rβ–$\gamma_c$ complex, despite their different receptor-binding chemistries. IL-15Rα substantially increased the affinity of IL-15 for IL-2Rβ, and this allostery was required for IL-15 *trans* signaling. Consistent with their identical IL-2Rβ–$\gamma_c$ dimer geometries, IL-2 and IL-15 showed similar signaling properties in lymphocytes, with any differences resulting from disparate receptor affinities. Thus, IL-15 and IL-2 induced similar signals, and the cytokine specificity of IL-2Rα versus IL-15Rα determined cellular responsiveness. Our results provide new insights for the development of specific immunotherapeutics based on IL-15 or IL-2.**



Interleukin 15 (IL-15) and IL-2 are four-helix bundle cytokines critical to the function and homeostasis of lymphocytes and natural killer (NK) cells. Despite their sparse sequence similarity (19% identity), both IL-2 and IL-15 form heterodimers with the receptor subunit IL-2Rβ and the common γ-chain ($\gamma_c$) to activate the pathways of the kinase Jak and STAT transcription factors; phosphatidylinositol-3-OH kinase (PI(3)K) and the kinase Akt; and the GTPase Ras and mitogen-activated protein kinase (MAPK)[1]. The receptor component $\gamma_c$ is additionally used and shared by IL-4, IL-7, IL-9 and IL-21 and is encoded by the gene mutated in humans with X-linked severe combined immunodeficiency[2]. In agreement with their use of common signaling receptors, IL-2 and IL-15 have several shared actions, such as stimulating the proliferation and cytotoxicity of cytotoxic T lymphocytes and NK cells[1]. However, these cytokines are not functionally redundant. Mice deficient in IL-2 or IL-15 have distinct phenotypes, and administration of IL-2 and IL-15 to mice and primates leads to divergent immunological outcomes[1,3]. Although both cytokines stimulate diverse lymphocyte and natural killer cell subsets, IL-2 favors the homeostasis of regulatory T cells and the regulation of the differentiation of helper T cells[4], whereas IL-15 favors the population expansion of $CD8^+$ memory cells, NK cells and NK T cells[1].

The molecular basis for the paradox of how IL-15 and IL-2 can both signal through IL-2Rβ and $\gamma_c$ but produce divergent functions remains controversial. Each cytokine has its own variably expressed α-receptor subunit (IL-2Rα (CD25) for IL-2 and IL-15Rα for IL-15), which results in much greater sensitivity of each cytokine for the intermediate-affinity receptor consisting of IL-2Rβ and $\gamma_c$ (ref. 1). In this context, IL-15 is 'enigmatic' in that it is dominantly presented in *trans* by IL-15Rα to IL-2Rβ and $\gamma_c$ on a neighboring cell; although IL-2 can also be presented in *trans*[5], it is more typically presented in *cis* to IL-2Rβ and $\gamma_c$ on the same cell surface[6]. Although neither IL-15Rα nor IL-2Rα is generally thought to have signaling functions, this distinct mode of presentation of the cytokines to the signaling receptors could potentially explain some aspects of the different *in vivo* functions of the cytokines. Thus, explanations for the different functions of IL-2 and IL-15 could involve *cis* versus *trans* presentation of the cytokines and/or differences in the expression of their α-receptor subunits, as well as unique temporal and spatial patterns of expression of the cytokines themselves, which could result in selective stimulation of some cell types rather than others. An alternative conjecture is that IL-2 and IL-15 may produce fundamentally different signals despite sharing common signaling receptors[7]. It is unclear from a structural perspective how IL-2 and IL-15 might transmit unique signals, although substantially divergent geometries of the dimeric receptors could, in principle, lead to different signaling outcomes, as has been speculated to occur for erythropoietin and other cytokines[8]. The crystal structure of the quaternary IL-2–IL-2Rα–IL-2Rβ–$\gamma_c$ complex has been reported[9], as has the binary complex of IL-15–IL-15Rα[10]. However, the absence of structural information for the complete quaternary IL-15 receptor ectodomain complex precludes conclusions about signaling differences that arise from structural differences. The various hypotheses to explain the distinct

[1]Howard Hughes Medical Institute, Stanford University School of Medicine, Stanford, California, USA. [2]Department of Molecular and Cellular Physiology, and Department of Structural Biology, Stanford University School of Medicine, Stanford, California, USA. [3]Laboratory of Molecular Immunology, National Heart, Lung, and Blood Institute, National Institutes of Health, Bethesda, Maryland, USA. [4]Department of Chemistry, Stanford University, Stanford, California, USA. Correspondence should be addressed to K.C.G. (kcgarcia@stanford.edu).

Received 6 July; accepted 11 September; published online 28 October 2012; doi:10.1038/ni.2449

**Table 1 Data collection and refinement statistics**

| | IL-15–IL-15Rα–IL-2Rβ–$\gamma_c$ |
|---|---|
| **Data collection** | |
| Space group | $P2_12_12_1$ |
| **Cell dimensions** | |
| *a*, *b*, *c* (Å) | 70.95, 74.61, 129.21 |
| $\alpha$, $\beta$, $\gamma$ (°) | 90.0, 90.0, 90.0 |
| Resolution (Å) | 40.23–2.35 (2.39–2.35) |
| $R_{sym}$ | 10.1 (65.6) |
| $I / \sigma I$ | 18.7 (2.3) |
| Completeness (%) | 99.2 (94.9) |
| Redundancy | 6.9 (5.5) |
| **Refinement** | |
| Resolution (Å) | 40.23–2.35 (2.39–2.35) |
| Reflections | 29,215 |
| $R_{work}$ / $R_{free}$ | 18.2/22.7 (24.2/32.8) |
| Atoms | |
| Protein | 4,704 |
| Ligand-ion | 92 |
| Water | 254 |
| B-factors | |
| Protein | 40.3 |
| Ligand-ion | 53.3 |
| Water | 39.5 |
| r.m.s. deviation | |
| Bond lengths (Å) | 0.004 |
| Bond angles (°) | 0.76 |

Shell of highest resolution is in parenthesis.

actions of IL-2 and IL-15, whether functionally or structurally derived, are not mutually exclusive, and the extent to which each contributes to the unique biological effects of IL-2 and IL-15 is unclear.

In this report we investigate several aspects of IL-15 structural and functional biology. First, we determined the crystal structure of the IL-15 quaternary complex to compare the molecular recognition strategies used by IL-15 and IL-2 in binding the shared IL-2Rβ and $\gamma_c$ subunits, as well as to assess the relative geometries of receptor heterodimerization induced by the two cytokines. Second, informed by those structural comparisons, we did molecular dynamics simulations and biophysical affinity measurements to probe the mechanism whereby IL-15Rα enhances the potency of IL-15. Finally, given the structural data indicating very similar receptor-binding modes, we characterized the signaling and gene-expression profiles of lymphocytes induced by IL-2 and IL-15 to assess whether these cytokines produce different intracellular signals that could explain their functional differences.

## RESULTS

### Comparison of the IL-15 and IL-2 quaternary complexes

Our initial attempts to determine the structure of the quaternary complex of IL-15 yielded crystals that diffracted to a resolution of only 3.8 Å. To obtain a structure of higher resolution, we did reductive methylation of the complex. This mild chemical modification results in dimethylation of surface lysine residues that can often improve crystal diffraction[11], and in this way we improved diffraction of the IL-15 quaternary receptor complex to 2.35 Å (**Table 1** and **Supplementary Figs. 1a–c** and **2a**). We determined the structure by molecular replacement using published models of IL-2Rβ, $\gamma_c$, IL-15 and IL-15Rα (refs. 9,10). The overall structure of the IL-15 quaternary complex (**Fig. 1a**) bears similarity to that of the two other $\gamma_c$-containing cytokine-receptor complexes reported so far, containing IL-2 and IL-4 (refs. 9,12). The IL-15 quaternary complex, containing its own α-receptor subunit and the shared signaling receptors IL-2Rβ and $\gamma_c$, assembles in a way nearly identical to that of the IL-2 quaternary complex (Protein Data Bank accession code, 2B5I; **Fig. 1b**), with IL-2Rβ binding to site I on the cytokine and $\gamma_c$ binding to site II. We were able to superimpose the structures of the IL-15 and IL-2 quaternary complexes with a root-mean-square deviation (r.m.s. deviation) of 1.18 Å (**Fig. 1b**), indicative of close structural similarity. In the signaling subunits IL-2Rβ and $\gamma_c$, the greatest differences between the IL-2 and IL-15 complexes are in slight repositioning of the D1 domains in contact with the cytokines. In contrast, the positions of the D2 domains, which form the receptor-receptor contacts and lead toward the cell surface, are nearly identical, which suggests that functional differences in signaling by IL-2 versus IL-15 are unlikely to be explained by alteration of the receptor architecture or dimer-angle geometry.

At the IL-2Rβ site I interface (**Fig. 2a**,**b**), IL-15 and IL-2 share sparse identity, with only three contact residues conserved (Asp8, Asp61 and Asn65 of IL-15; and Asp20, Asp84 and Asn88 of IL-2) among the fifteen residues that contact IL-2Rβ (**Fig. 2c**). In an example of convergent structural evolution, these three residues are not conserved in linear sequence but instead are conserved in their three-dimensional spatial locations on the cytokine helices that form the receptor-binding interface (**Fig. 2c**). They make identical contacts with IL-2Rβ: Asp8 forms hydrogen bonds to His133 and Tyr134 of IL-2Rβ; Asp61 forms a salt bridge with Lys71; and Asn65 contacts the triad of Arg42, Gln70 and Tyr134. The importance of these residues for both IL-2 and IL-15 has been confirmed by mutagenesis studies[13–16]. Of the remaining site I contact residues in IL-15, many are relatively conservative substitutions of those in IL-2 and interact with IL-2Rβ in a similar way. For example, Val91 and Ile92 of IL-2 form van der Waals interactions with Thr73 and Val75 of IL-2Rβ; in IL-15, the same contacts are made by Ile68 and Lys69. However, there are some notable differences in the binding chemistry of the IL-2–IL-2Rβ and IL-15–IL-2Rβ interfaces. IL-2 recognizes Glu136 of IL-2Rβ through a hydrophobic interaction between Leu19 and the aliphatic portion of the glutamic acid side chain (**Fig. 2b**). In the IL-15 site I interface, this interaction has a completely different character, as Glu136 forms a

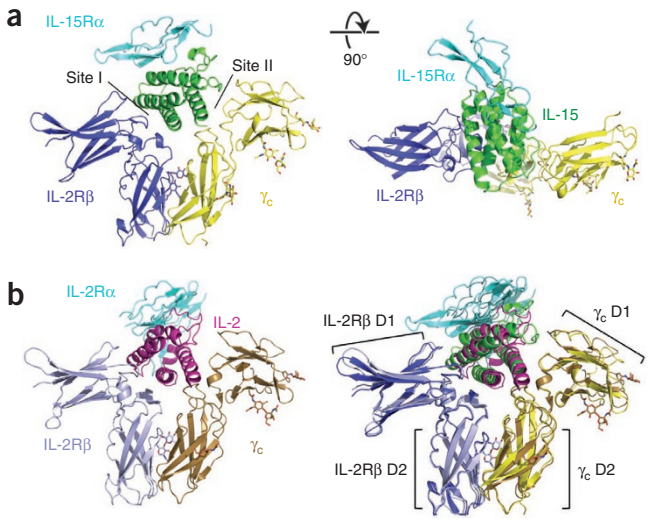


**Figure 1** The crystal structure of the quaternary IL-15 receptor complex. (**a**) Front view (left) and top view (right) of the IL-15 quaternary receptor complex composed of IL-15 (green), IL-15Rα (cyan), IL-2Rβ (blue) and $\gamma_c$ (gold), including the site I and site II interactions of IL-15 with IL-2Rβ and $\gamma_c$, respectively (left). (**b**) The structure of the IL-2 quaternary complex (Protein Data Bank accession code 2B5I; left), and superimposition of the IL-15 and IL-2 receptor complexes (right; r.m.s.d., 1.175 Å).

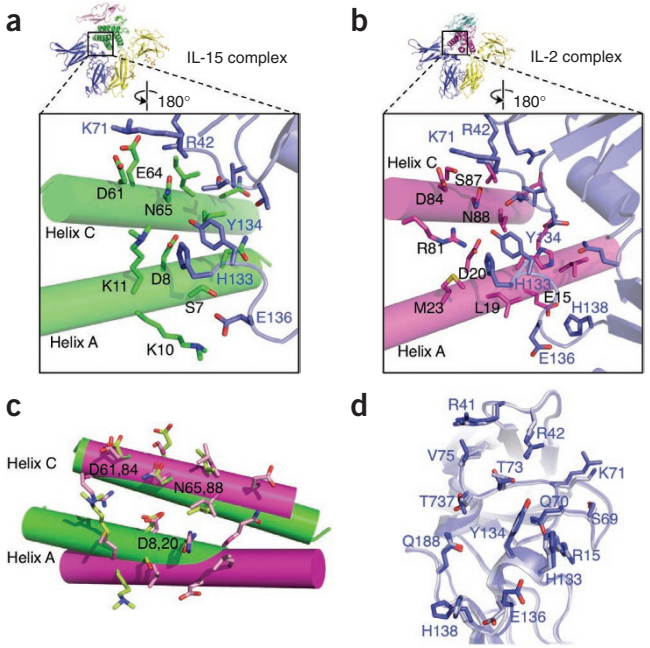


**Figure 2** Comparison of the site I interfaces of IL-15 and IL-2. (**a**) The site I interface of IL-15 (green cylinders and side chains) in contact with IL-2Rβ (blue loops and side chains). (**b**) The site I interface of IL-2 (magenta cylinders and side chains) in contact with IL-2Rβ (blue loops and side chains). (**c**) Superimposition of the A and C helices of IL-15 (green) and IL-2 (magenta), showing structural conservation of Asp61, Asn65 and Asp8 of IL-15. (**d**) Superimposition of IL-2Rβ bound to IL-15 (light blue) and IL-2 (blue), indicating the apparent rigidity of the interface in binding two distinct cytokines.

hydrogen bond with Ser7 of IL-15 (**Fig. 2a**). Another salient feature of the IL-15–IL-2Rβ interaction is the lysine pair Lys10 and Lys11. Lys10 forms a salt bridge with Glu136 of IL-2Rβ that has no equivalent in IL-2, whereas Lys11 seems to satisfy the role of two IL-2 residues at the site I interface. Pointing upward from helix A toward helix C, Lys11, like Met23 of IL-2, presents the aliphatic portion of its side chain for van der Waals interactions with His133 of IL-2Rβ while positioning its terminal amine at the same site as the guanidinium of Arg81 of IL-2 (**Fig. 2a–c**). Thus, whereas the three key contact residues in the interface are maintained in IL-2 and IL-15, the overall divergence of the IL-2Rβ-binding chemistry suggests that cytokine-specific strategies to disrupt or enhance the binding of IL-2 versus that of IL-15 would be feasible in an engineered protein therapeutic.

Despite the sequence dissimilarity and the unique binding strategies of the IL-2Rβ ligands IL-2 and IL-15, the conformation of the side chains and binding loops of IL-2Rβ are nearly indistinguishable when in complex with either cytokine. Of the 14 residues in contact with either IL-2 or IL-15, only two residues show substantial changes in position or rotameric conformation (**Fig. 2d**). The apparent rigidity of the IL-2Rβ interface, despite its cross-reactivity with many cytokines, is reminiscent of the shared cytokine receptor gp130 and suggests that as for gp130, the mechanism of degenerate cytokine recognition by IL-2Rβ is not driven by conformational plasticity[17]. Instead, the receptor seems to have evolved a rigid interface that accommodates diverse energetic binding solutions reminiscent of those of other cross-reactive immunological receptors such as NKG2D[18].

At its site II interface, IL-15 binds to $\gamma_c$ through a rather chemically 'featureless' interface, in contrast to the highly polar and specific side-chain contacts in the site I interface. Although the IL-15 interaction has some unique features, a similar docking strategy is used for the binding of $\gamma_c$ to IL-2 and IL-4, and this emphasizes the cross-reactive properties of the $\gamma_c$ cytokine-binding surface, which is able to engage all members of the $\gamma_c$ cytokine family. In particular, the absence of highly charged bonds would facilitate degenerate cytokine binding. Like IL-2 and IL-4 (data not shown), IL-15 interacts with the EF1, BC2 and FG2 loops of $\gamma_c$ by side chains positioned by the A and D helices (**Fig. 3a,b**). In a similar example of the three-dimensional structural mimicry of site I, the most critical 'hot-spot' residue Gln126 of IL-2 is conserved in IL-15 as Gln108 and packs neatly into the same trench of $\gamma_c$ formed by residues Pro207, Cys209, Gly210 and Ser211. Similarly, Tyr103 of $\gamma_c$, which is mutant in some people with X-linked severe combined immunodeficiency and is critical for optimal ligand binding, is recognized by parallel mechanisms in IL-2 and IL-15; the phenyl ring packs with Ser127 of IL-2 and Met109 of IL-15, whereas the hydroxyl moiety makes a hydrogen bond to Ser130 of IL-2 and Asn112 of IL-15.

IL-15 (108 residues) is smaller than IL-2 (133 residues), and a distinct structural feature in site II seems to have evolved to compensate for this difference. In the site II interface of IL-15, there is an additional region of contact between residues on the A-B loop of IL-15 and the CC'1 loop of $\gamma_c$ (**Fig. 3a,c,d**). This interface buries an area of 490Å$^2$, which constitutes over one third of the entire buried surface area of the site II interface of IL-15 (1367Å$^2$). IL-2 forms a much smaller interface with this region of $\gamma_c$, contributing only 70Å$^2$, or 7%, of the 995Å$^2$ of total buried surface area of site II (**Fig. 3d**). IL-15 has shorter A and D helices than does IL-2 (2 turns and 1.5 turns

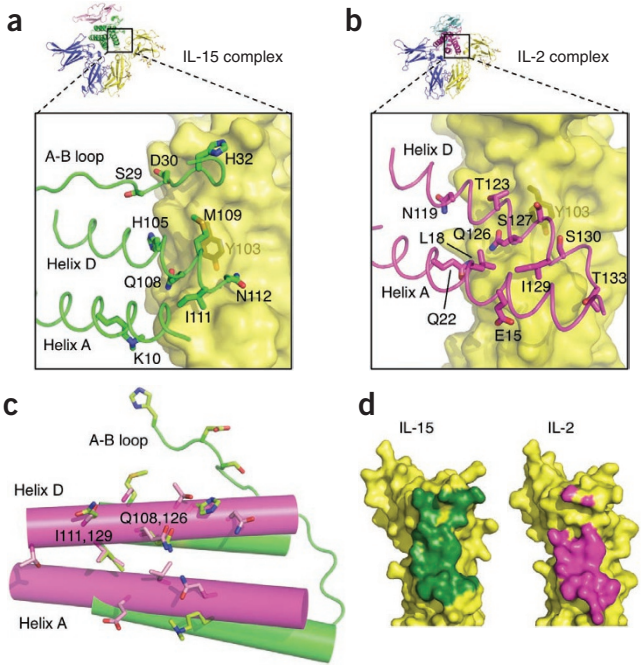


**Figure 3** Comparison of the site II interfaces of IL-15 and IL-2. (**a**) The site II interface of IL-15 (green tubes and side chains) bound to $\gamma_c$ (gold surface). Dark yellow indicates Tyr103 of $\gamma_c$ (residue associated with X-linked severe combined immunodeficiency). (**b**) The site II interface of IL-2 (magenta tubes and side chains) bound to $\gamma_c$ (gold surface). (**c**) Superimposition of the A and D helices of IL-15 (green) and IL-2 (magenta). Only Gln108 and Ile111 of IL-15 are strictly conserved at the interface. (**d**) Binding interfaces on the surface of $\gamma_c$, shaded according to binding to IL-15 (left; dark green) or IL-2 (right; magenta).

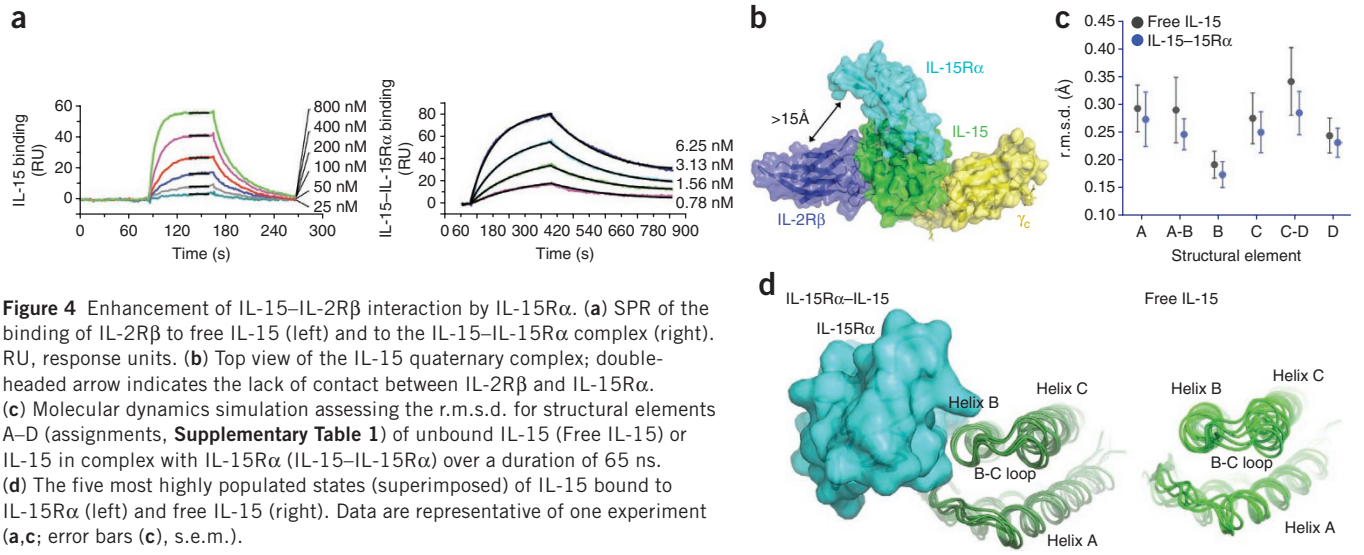


**Figure 4** Enhancement of IL-15–IL-2Rβ interaction by IL-15Rα. (**a**) SPR of the binding of IL-2Rβ to free IL-15 (left) and to the IL-15–IL-15Rα complex (right). RU, response units. (**b**) Top view of the IL-15 quaternary complex; double-headed arrow indicates the lack of contact between IL-2Rβ and IL-15Rα. (**c**) Molecular dynamics simulation assessing the r.m.s.d. for structural elements A–D (assignments, **Supplementary Table 1**) of unbound IL-15 (Free IL-15) or IL-15 in complex with IL-15Rα (IL-15–IL-15Rα) over a duration of 65 ns. (**d**) The five most highly populated states (superimposed) of IL-15 bound to IL-15Rα (left) and free IL-15 (right). Data are representative of one experiment (**a**,**c**; error bars (**c**), s.e.m.).

shorter, respectively) and consequently makes fewer contacts with $\gamma_c$ from those helices. Although IL-2 has ten contact residues located between those two helices, IL-15 has only five. Furthermore, IL-15 binds to $\gamma_c$ with considerably lower shape complementarity than does IL-2 or IL-4 (0.59 for IL-15; 0.84 for IL-2; and 0.82 for IL-4). Thus, a potential explanation for the unique contacts of IL-15 with the $\gamma_c$ CC'1 loop would be that the interface serves to have compensated for the missing A and D helical contacts present in other $\gamma_c$ cytokines, as well as the less favorable shape complementarity if IL-15 with $\gamma_c$.

In conclusion, IL-15 assembles the IL-2Rβ–$\gamma_c$ signaling complex in a way nearly indistinguishable from that of IL-2, despite their shared and unique molecular recognition strategies in binding the receptor subunits. The great overall similarity of the structures of the IL-15 and IL-2 complexes disfavors structural explanations for the unique functional properties of the cytokines. However, the details of the cytokine and receptor contacts present structural opportunities for the specific disruption or enhancement of either cytokine for therapeutic purposes.

## Molecular insight into IL-15 *trans* signaling

Signaling through the receptors for IL-2 and IL-15 is initiated when IL-2Rα or IL-15Rα captures IL-2 or IL-15, respectively, and presents the cytokine to IL-2Rβ and $\gamma_c$. IL-15, however, can signal through an unusual mechanism whereby it is presented in *trans* by cells expressing IL-15 and IL-15Rα to IL-15-responsive cells expressing IL-2Rβ and $\gamma_c$ (ref. 19). Unlike the situation in *cis*, IL-15 *trans* signaling does not benefit from the substantial surface-capture effect of the binding of IL-15Rα to IL-15 on the same cell, as is the case for IL-2. A major role for IL-2Rα is simply to enrich the cell surface by capturing IL-2 from solution, which results in a much lower entropic barrier for the binding of IL-2 to IL-2Rβ and $\gamma_c$. As IL-15 is presented in *trans*, it does not enjoy this mechanistic advantage, which raises the question of how IL-15Rα effectively enhances IL-15 activity. Nevertheless, *trans* presentation has proven to be a major mechanism of IL-15 action *in vivo*[6], which suggests that IL-15Rα may have other IL-15-sensitizing functions in addition to surface capture. IL-15 in complex with soluble IL-15Rα has greater biological activity than does free IL-15 on some cell types[20–22]. Salient to this point is that IL-2 undergoes a small conformational change after binding to IL-2Rα in the region of the IL-2 C-helix in contact with IL-2Rβ (ref. 23). Furthermore, mutant IL-2 'superkines' (such as super-2 or H9) that stabilize the C helix enhance the affinity of IL-2 for IL-2Rβ by nearly 300-fold (ref. 24). As IL-15 would not benefit from the entropic gain that results from *cis* surface capture by IL-15Rα, as does IL-2, we sought to determine to what extent IL-15Rα induces affinity enhancement of IL-15 for IL-2Rβ through *trans* capture and presentation. We measured the affinity of both free and IL-15Rα-bound IL-15 for immobilized IL-2Rβ by surface plasmon resonance (SPR). Free IL-15 bound to IL-2Rβ with a dissociation constant of 438 nM (**Fig. 4a**), consistent with published SPR measurements for this interaction[25]. Notably, IL-15–IL-15Rα complex bound to IL-2Rβ with a dissociation constant of 3 nM (**Fig. 4a**), an affinity approximately 150-fold greater than that of free IL-15.

The structure of the quaternary IL-15 complex does not offer an obvious explanation for how IL-15Rα influences the interaction between IL-15 and IL-2Rβ. Notably, IL-15Rα does not contact IL-2Rβ, with a distance of >15Å separating the subunits at their closest point (**Fig. 4b**). However, the conformational mechanisms of this allostery may be dynamic and subtle and might not be observable in a static crystal structure. Structural alignment of the binary IL-15 complex (Protein Data Bank accession code, 2Z3Q) and quaternary IL-15 complex indicated that the IL-15–IL-15Rα complex does not undergo a substantial conformational change after binding IL-2Rβ and $\gamma_c$ (r.m.s. deviation, 0.453Å; **Supplementary Fig. 2b**). Therefore, we hypothesized that IL-15Rα might thus stabilize a conformation of IL-15 that is more able to bind IL-2Rβ, akin to the effect of IL-2Rα for IL-2. Direct comparison of free and IL-15Rα-bound IL-15 is not possible at present, as the structure of free IL-15 has yet to be elucidated, possibly because of the biochemical instability of the molecule in the absence of IL-15Rα[20]. We instead turned to computational approaches to investigate the potential structural and dynamics influences of IL-15Rα on IL-15.

Proteins exist in solution as flexible conformational ensembles whose equilibrium can be perturbed after ligand binding. For example, IL-2 has been shown to be very conformationally plastic[26]. Using molecular dynamics simulations, we sought to determine how binding to its α-receptor subunit alters the conformational ensemble of IL-15. We constructed an atomically detailed Markov-state model (MSM) to directly probe the relative conformational flexibility of IL-15 when free in solution or when bound to the α-receptor subunit. The states in this MSM come from the kinetic clustering of rapidly interconverting conformations that result from atomistic simulations[27]. Each of these metastable states corresponds to a local minimum in the underlying

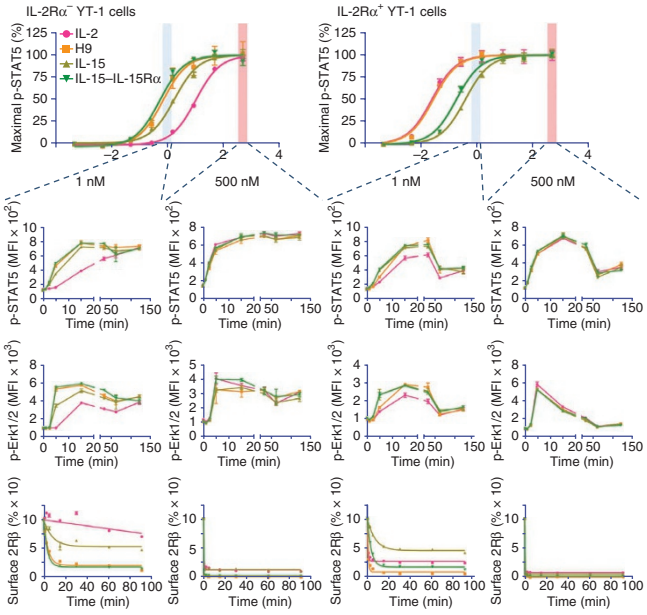


**Figure 5** Analysis of signaling by IL-2 and IL-15 in YT-1 human NK cells. Dose-response relationships of phosphorylated (p-) STAT5 with IL-2, H9, IL-15 and IL-15–IL-15Rα complexes in IL-2Rα⁻ YT cells (top left) and IL-2Rα⁺ YT cells (top right); signaling kinetics relationships for phosphorylated STAT5 (second row) or Erk1/2 (third row); and internalization kinetics of IL-2Rβ (presented relative to maximal surface expression; bottom row). Horizontal axes of top row indicate the log of cytokine concentration in nM; all kinetics experiments (rows below) used a saturating concentration (500 nM) or subsaturating concentration (1 nM) of each cytokine. MFI, mean fluorescent intensity. Data are representative of at least two experiments per panel (error bars, s.e.m. of triplicates).

free-energy landscape that ultimately determines the system's structure and dynamics. Using these MSMs, we calculated the average r.m.s. deviation for each structural element under the two conditions (**Fig. 4c**). This analysis showed that the conformational freedom of the A-B and C-D loops was greatly restricted in the bound state, as expected, given that these loops form the contacts to IL-15Rα. To a lesser extent, there seemed to be global stabilization of the four helices. Visualization of the most highly populated conformations from each set of conditions showed that the differences were subtle, both in the helices and loops (**Fig. 4d**). This was in contrast to IL-2, for which binding of IL-2Rα specifically repositions the B and C helices of IL-2 for optimal binding to IL-2Rβ[23,24]. Despite such disparate mechanisms (global versus helix-specific stabilization), our results suggested that IL-15Rα and IL-2Rα share the property of conformationally stabilizing relatively flexible cytokine ligands to decrease energetic barriers to binding and increase the affinity of IL-15 and IL-2 for IL-2Rβ.

## Comparison of IL-15 and IL-2 signaling properties

There is considerable controversy about whether IL-2 and IL-15 yield different intracellular signals after activation of the receptor. Although some studies have found that the cytokines produce indistinguishable signaling profiles[28], others have demonstrated substantial differences. These differences have been reported to be alterations in signaling kinetics[29,30] and efficacy[31] for individual pathways. Given the considerable structural similarity of the quaternary complexes of IL-2 and IL-15, we sought to reexamine their membrane-proximal signaling activities. For this, we determined the dose-response relationships and signaling kinetics of IL-2 and IL-15 on cells expressing or deficient in IL-2Rα and IL-15Rα. We took advantage of the human NK cell line YT-1, which we sorted into separate IL-2Rα⁺ and IL-2Rα⁻ subpopulations (**Supplementary Fig. 3a**) for dose-response and kinetic analysis of the phosphorylation of the transcription factor STAT5 and kinase Erk, as assayed by flow cytometry with phosphorylation-specific antibodies (**Fig. 5**). We also isolated CD8⁺ T cells from mouse spleens and assayed phosphorylation of STAT5 and the ribosomal protein S6 (S6R; a component of the PI(3)K signaling pathway) in response to cytokine treatment of freshly isolated cells and cells prestimulated with antibody to CD3 (anti-CD3; **Fig. 6**). Whereas prestimulated CD8⁺ cells had moderate to high expression of both α-receptor subunits, freshly isolated CD8⁺ cells did not express IL-2Rα and had only a modest expression of IL-15Rα (**Supplementary Fig. 3b**). To further isolate effects-mediated by the α-receptor subunits, we used IL-15–IL-15Rα complexes and the IL-2 'superkine' H9 (which has such high affinity for IL-2Rβ that it can potently induce signaling through the IL-2Rβ–$\gamma_c$ heterodimer on IL-2Rα⁻ cells), in addition to free IL-15 and wild-type IL-2 (ref. 24).

On YT-1 cells lacking IL-2Rα, the effector concentration for a half-maximal response ($EC_{50}$) for signaling for each cytokine correlated with its relative affinity for IL-2Rβ, with the rank order for $EC_{50}$ values being IL-15–IL-15Rα = H9 < IL-15 < IL-2 (**Fig. 5**, top left). The somewhat lower $EC_{50}$ value of IL-15 than that of IL-2 may have resulted from the small amount of IL-15Rα expressed on YT-1 cells (**Supplementary Fig. 3a**). When IL-2Rα was present, the $EC_{50}$ rank order was H9 = IL-2 < IL-15–IL-15Rα < IL-15, which reflected the surface-capture and avidity effects of membrane-bound IL-2Rα on IL-2 and H9 (**Fig. 5**, top right). We obtained similar results when we compared the dose-response relationships of freshly isolated and preactivated mouse CD8⁺ cells, but with a few distinctions. On freshly isolated CD8⁺ cells, free IL-15 produced a biphasic dose-response relationship, consistent with the low expression of IL-15Rα in these cells, including a high proportion of IL-15Rα⁻ cells (**Fig. 6**, top left, and **Supplementary Fig. 3b**). Notably, IL-15–IL-15Rα complexes did not demonstrate a biphasic dose-response curve, suggestive of the ability of soluble IL-15Rα to impede engagement of membrane-bound IL-15Rα. The subsequent rank order of $EC_{50}$ values was IL-15 ($EC_{50}$ value 1) < H9 < IL-15–IL-15Rα< IL-15 ($EC_{50}$ value 2) = IL-2. On preactivated CD8⁺ cells, the curves for the $EC_{50}$ values of IL-2 and IL-15 shifted substantially to the left (**Fig. 6**, top right), which reflected the potent effect of the expression of IL-2Rα and IL-15Rα on cytokine sensitivity. The curve for H9 also shifted to the left, as it is able to bind IL-2Rα and benefits from surface capture, but the $EC_{50}$ value of the IL-15–IL-15Rα complex was essentially unchanged relative to that of freshly isolated cells. For all cells and regardless of differences in $EC_{50}$ values, IL-2, H9 and the IL-15–IL-15Rα complex stimulated equivalent phosphorylation of STAT5, Erk and S6R at saturating doses.

We next monitored the kinetics of signaling by IL-2 and IL-15 with subsaturating doses (1 nM or 20 pM) and saturating doses (500 nM or 10 nM) of IL-2, H9, IL-15 and IL-15–IL-15Rα complexes. We assayed the three main IL-2 and IL-15 signaling pathways (Jak-STAT, Ras-MAPK and PI(3)K-Akt) and found their signaling kinetics were very much dependent on concentration and α-receptor subunit (**Figs. 5** and **6**, middle and bottom). In particular, both the rate and magnitude of signaling for each pathway were readily predicted by their respective concentration-response relationships. For example, at subsaturating concentrations and in the absence of IL-2Rα, IL-2 had the slowest signaling kinetics of all the cytokines, which matched its right-shifted dose-response curve under those conditions

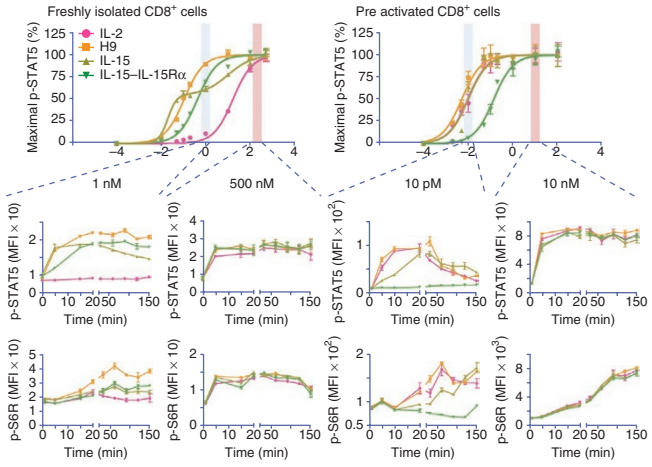


**Figure 6** Analysis of signaling by IL-2 and IL-15 in primary mouse CD8$^+$ cells. Dose-response relationships (as in **Fig. 5**) of phosphorylated STAT5 with IL-2, H9, IL-15 and IL-15–IL-15Rα complexes in freshly isolated CD8$^+$ T cells (top left) and CD8$^+$ T cells preactivated with anti-CD3 (top right), and signaling kinetics relationships for phosphorylated STAT5 (second row) and phosphorylated S6R (bottom row) at a saturating concentration (500 nM or 10 nM) or subsaturating concentration (1 nM or 10 pM) of each cytokine. Data are representative of two experiments (error bars, s.e.m. of duplicates).

(**Figs. 5** and **6**, far left). We noted a similar trend for the IL-15–IL-15Rα complexes on preactivated cells at subsaturating conditions (**Fig. 6**, middle left). In contrast, all four stimuli produced overlapping and nearly identical kinetic profiles for the phosphorylation of STAT5, Erk and S6R at saturating cytokine concentrations (**Figs. 5** and **6**, middle left and far right). Consistent with the kinetic phosphorylation profiles reported above, downregulation of the signaling receptor IL-2Rβ also demonstrated a strong relationship with cytokine affinity and concentration (**Fig. 5**, bottom). Specifically, the cytokines with higher affinity drove faster and more complete internalization of IL-2Rβ at lower cytokine concentrations, but the differences were diminished at saturating doses. Together these results indicated that IL-2 and IL-15 generated very similar, if not identical, intracellular signals after we accounted for variability in expression of the α-receptor subunit and cytokine-receptor affinity.

## IL-2 and IL-15 induce similar gene-expression profiles

As with intracellular signaling, differences in the gene expression induced by IL-2 and IL-15 have been reported[31,32], which perhaps account in part for functional differences between these two cytokines. We wondered if these differences, like the reported differences in membrane-proximal signaling, could be explained by concentration-dependent effects, or if the two cytokines produce fundamentally different gene-expression profiles. To maximize our chances of detecting genes regulated differently by IL-2 and IL-15, we used RNA sequencing to compare the gene-expression profiles of CD8$^+$ T cells stimulated with subsaturating cytokine concentrations commonly used by other investigators in the field (1 nM) or saturating concentrations of each cytokine (500 nM). Two-dimensional multidimensional scaling plot analysis showed that IL-2- and IL-15-regulated mRNA correlated at each time point and concentration (**Supplementary Fig. 4a**). As noted for the membrane-proximal signaling induced by IL-2 and IL-15, the gene-expression profiles elicited by these cytokines were more similar when the cytokines were applied at saturating concentrations ($r^2$ = 0.909 and 0.962 at 4 and 24 h, respectively; **Fig. 7a**, bottom) than when they were applied at subsaturating concentrations ($r^2$ = 0.784 and 0.611 at 4 and 24 h, respectively; **Fig. 7a**, top). To identify IL-2- and IL-15-regulated genes, we chose those with over five reads per kilobase of exon model per million mapped reads that also had a change in expression of twofold or more at any time point relative to their expression in unstimulated control cells. This analysis identified 4,690 genes regulated by IL-2 and 4,776 genes regulated by IL-15; many of the same genes were regulated by both cytokines, so a total of 5,182 different genes were regulated by at least one of these cytokines (**Supplementary Fig. 4b**). There was similar expression of 90.5% of the IL-2-regulated genes and 92.2% of the IL-15-regulated genes after stimulation with IL-2 or IL-15 (difference in expression of less than twofold). In contrast, 406 genes were more potently regulated by IL-2 than by IL-15 (ratio of expression after stimulation with IL-2 to expression after stimulation with IL-15, >2), and 492 genes were regulated more potently by IL-15 than by IL-2 (**Fig. 7b–d**, **Supplementary Fig. 4b** and **Supplementary Spreadsheets 1** and **2**).

Having identified candidate genes that may be regulated differently by IL-2 and IL-15, we sought to confirm the gene-expression differences

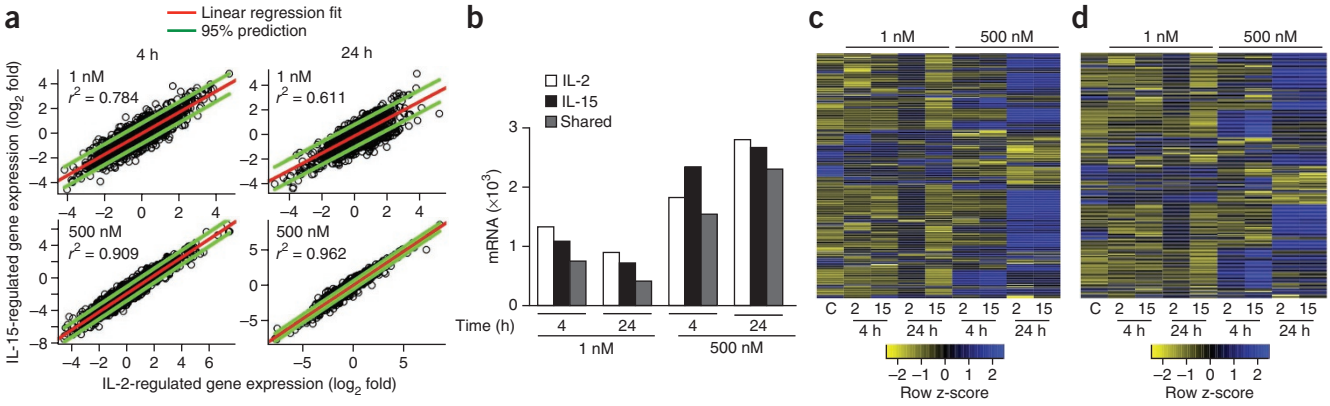


**Figure 7** RNA-sequencing analysis of gene transcription regulated by IL-2 and IL-15. (**a**) Correlations in the change in expression (log$_2$ fold) of IL-2- and IL-15-regulated genes with IL-2 and IL-15 at a concentration of 1 nM or 500 nM and at 4 h or 24 h after cytokine stimulation (95% confidence intervals not presented, as they almost overlap with the 95% prediction from the linear regression fit). (**b**) Quantification of genes regulated by IL-2 and/or IL-15 at 4 h or 24 h after cytokine stimulation and with IL-2 and IL-15 at a concentration of 1 nM or 500 nM. (**c**,**d**) Heat map of genes 'preferentially' regulated by IL-2 (**c**) or IL-15 (**d**); gene expression is normalized to the same range for each gene (–2 to 2; key). Data are representative of two independent experiments.

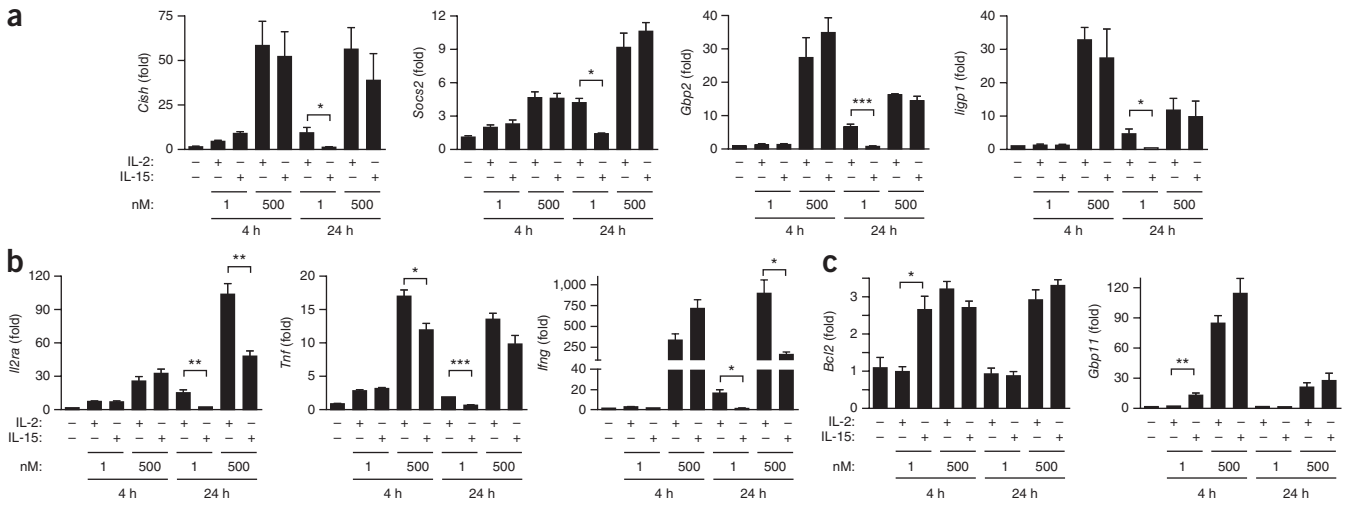


**Figure 8** Confirmation of differences in the regulation of IL-2 and IL-15 target genes. (**a**) Quantitative PCR analysis of expression of the cytokine-inducible genes *Cish* and *Socs2*, and *Gbp2* (which encodes guanylate-binding protein 2) and *Iigp1* (which encodes an interferon-inducible GTPase 1), in CD8$^+$ T cells at 4 h or 24 h after induction by IL-2 or IL-15 at a concentration of 1 nM or 500 nM. (**b**) Quantitative PCR analysis of the expression of *Il2ra*, *Tnf* and *Ifng* in CD8$^+$ T cells treated as in **a**. (**c**) Quantitative PCR analysis of the expression of *Bcl2* (which encodes the antiapoptotic protein Bcl-2) and *Gbp11* (which encodes a guanylate-binding protein) in CD8$^+$ T cells treated as in **a**. For all quantitative PCR, cDNA was generated from 150 ng total RNA, and equal amounts of input cDNA were further normalized based on the change-in-threshold ($\Delta C_T$) values of PCR with *Rpl7* primers (*Rpl7* is a control gene that encodes a ribosomal protein), and results are presented relative to expression in unstimulated (control) samples. $^*P \leq 0.05$, $^{**}P \leq 0.01$ and $^{***}P \leq 0.001$ (unpaired *t*-test). Data are representative of two independent experiments. (error bars, s.e.m. of triplicates).

and determine if they persisted independently of concentration. Thus, we stimulated CD8$^+$ T cells with a subsaturating concentration (1 nM) or saturating concentration (500 nM) of each cytokine and assayed by quantitative RT-PCR the expression of a set of genes at early (4 h) and late (24 h) time points. As we observed by RNA sequencing, at a concentration of 1 nM, IL-2 and IL-15 induced significant differences in gene expression at both time points (**Fig. 8**). However, when we applied saturating concentrations of each cytokine, the expression converged for most of the genes assayed (**Fig. 8a**,**c**). Some differences persisted at high concentration, as IL-2 induced higher expression of *Il2ra* (which encodes IL-2Rα), *Tnf* (which encodes the cytokine tumor-necrosis factor) and *Ifng* (which encodes interferon-γ) than did IL-15, even at high concentration (**Fig. 8b**). These differences were relatively modest, however, and ranged from less than 0.5-fold for *Tnf* to approximately 3-fold for *Ifng*. Thus, in parallel with their membrane-proximal signaling activity, IL-15 and IL-2 stimulated very similar transcriptional profiles, particularly when we accounted for cytokine concentration and expression of the α-receptor subunit.

## DISCUSSION

Since the initial discovery of IL-15 almost 20 years ago, many mechanisms have been offered to explain how IL-2 and IL-15 can produce divergent functional effects despite sharing common signaling receptors. In this work we have reported the X-ray crystal structure of the quaternary complex of IL-15 bound to the ectodomains of IL-15Rα, IL-2Rβ and $\gamma_c$; we found the complex to have a heterodimeric IL-2Rβ–$\gamma_c$ architecture approximately identical to that of the IL-2–IL-2R quaternary complex. The lack of substantial deviation between the signaling complexes of IL-2 and IL-15 in dimer topology suggested that any functional differences between the two cytokines would be unlikely to arise from 'instructive' extracellular structural influences. However, differences in the cytokine-interaction affinities and kinetics of the association of the respective cytokines with the IL-2Rβ and $\gamma_c$ extracellular domains could result in overall complex stability differences that would be manifested as distinct signaling outcomes. Thus, through the use of flow cytometry with phosphorylation-specific antibodies, we compared signaling mediated by IL-2 and IL-15 over a broad range of cytokine concentrations and kinetic intervals and found that many of the apparent signaling differences between IL-2 and IL-15 could be explained by differences between the two cytokines in receptor affinity. Similarly, we found high correlation in the gene-expression profiles of cells stimulated with IL-2 and IL-15 and that differences in gene expression were generally lower at saturating concentrations of the cytokines. When differences persisted at saturation, they remained modest, which brought into question their true biological relevance. Although our results do not rule out the possibility of additional mechanisms of IL-15 action, they indicate that these mechanisms are not necessary to explain the complex and diverse functions of IL-15 and IL-2 observed *in vivo*. Instead, we found that the expression of the α-receptor subunit and cytokine concentration substantially affected the signaling activity of IL-2 and IL-15 and produced differences in gene expression when the cytokines were at different points on their respective concentration-response curves. Presumably the disparate spatial and temporal expression of the α-receptor subunits, as well as their absolute expression, dynamically regulates the sensitivity of cells for each respective cytokine and their ensuing response to stimulation.

Underscoring the importance of their respective α-receptor subunits in their functions is the notable difference between IL-2 and IL-15 in the way they are presented to effector cells. As IL-15 binds to IL-15Rα with extremely high affinity and IL-15Rα is widely expressed in tissues, IL-15 is believed to exist in the body mainly in a complex with IL-15Rα and is therefore primed for *trans* presentation to cells that express IL-2Rβ and $\gamma_c$ (ref. 6). As mentioned before, soluble complexes of IL-15–IL-15Rα that mimic *trans* presentation have greater potency than does free IL-15 (refs. 20–22) Through our studies we have elucidated the mechanism underlying this phenomenon; we found that binding of IL-15Rα increased the affinity of IL-15 for IL-2Rβ approximately 150-fold. This affinity increase for

IL-2Rβ subsequently manifested as a left shift in the concentration-response relationship of IL-15 signaling in cells that lacked IL-15Rα. The structural basis for the affinity enhancement of IL-15 for IL-2Rβ seemed to be a consequence of a much greater degree of global stabilization of IL-15 after it bound to IL-15Rα than of IL-2 after it binds to IL-2Rα[23,24]. From a teleological perspective, the affinity enhancement endowed by IL-15Rα onto the IL-15–IL-2Rβ interaction may serve to compensate for the lack of surface capture in the setting of *trans* presentation.

IL-2 is administered clinically as immunotherapy for the treatment of renal cell carcinoma and metastatic melanoma. However, IL-2 therapy is hampered by dose-limiting toxicity from vascular leakage and the counterproductive activation of regulatory T cells that abrogate antitumor responses. Both of these undesirable side effects are attributable to the activation of cells that express IL-2Rα: pulmonary vascular endothelial cells and IL-2Rα$^+$CD4$^+$ regulatory T cells[33,34]. IL-2 variants that bind to IL-2Rβ with high affinity independently of IL-2Rα (super-2 or H9) have greater antitumor efficacy and result in less pulmonary edema than does wild-type IL-2 (ref. 24). Super-2 activates antitumor responses from IL-2Rα$^-$ cells such as naive T cells and NK cells more efficiently, with proportionally less activation of IL-2Rα$^+$ cells such as regulatory T cells and pulmonary endothelial cells, than does wild-type IL-2. The potential use of IL-15 for the treatment of cancer has been met with considerable enthusiasm, and it is now undergoing evaluation in phase I clinical trials (trial NCT01021059 of the National Cancer Institute). Notably, IL-15 does not cause vascular leak syndrome or stimulate regulatory T cells but 'preferentially' activates cytotoxic T lymphocytes and NK cells thought to mediate antitumor effects[3], in many ways similar to super-2. Similarly, a single-chain fusion protein of IL-15 and IL-15Rα (RLI) has been proposed as a potential antitumor agent with greater potency and bioavailability than free IL-15 (ref. 35).

In comparisons of the therapeutic antitumor potentials of IL-2 and IL-15 and their respective variants (super-2 and IL-15–IL-15α complexes), the degree of dependence on the α-receptor subunit inherent in each molecule must be considered. Although IL-2 and IL-15 represent the extreme ends of the spectrum, showing great dependence on their α-receptor subunits for potency, super-2 and RLI seem to have a dependence between that of the two wild-type cytokines, showing little to no 'preference' for cells that express IL-2Rα or IL-15Rα. Super-2 and RLI can be further distinguished by their interactions with IL-2Rα and IL-15Rα. As the IL-15Rα-binding site is sterically obscured in RLI, it represents the exact midpoint between IL-2 and IL-15 on the spectrum, unaffected by the presence or absence of either α-receptor subunit. In contrast, super-2 is able to bind to IL-2Rα and consequently shows some 'preference' for IL-2Rα$^+$ cells rather than IL-2Rα$^-$ cells, albeit to a much lower degree than does wild-type IL-2. This subtle distinction may yield notable differences in efficacy and toxicity. For example, though IL-2Rα is responsible for many of the undesirable side effects of IL-2, some IL-2Rα$^+$ cells (such as activated T cells) may be beneficial to target. Similarly, IL-15Rα$^+$ cells (such as NK cells and cytotoxic CD8$^+$ cells) are critical determinants of antitumor efficacy *in vivo*.

Given the considerations noted above, it may be possible to enhance immunotherapy with IL-2 and/or IL-15 by modulating their dependence on IL-2Rα and IL-15Rα, respectively, thus 'tuning' the distribution of cells of the immune system activated for therapeutic effect. In this context, super-2 and RLI represent good starting points for such immunological manipulation. Just as the structure of the IL-2 quaternary complex enabled the engineering of super-2, we hope to leverage the information obtained from the IL-15 quaternary complex presented here for the design of improved IL-15 therapies.

## METHODS

Methods and any associated references are available in the online version of the paper.

**Accession codes.** Protein Data Bank: atomic coordinates and structure factors, 4GS7; GEO: IL-2 and IL-15 RNA sequencing data, GSE40350.

*Note: Supplementary information is available in the online version of the paper.*

ACKNOWLEDGMENTS

We thank E. Long, M. Rubinstein and members of the Leonard and Garcia laboratories for advice and discussions; and N. Goriatcheva, D. Waghray and S. Fischer for technical assistance. Supported by the US National Institutes of Health (R01 AI51321 to K.C.G.; R01 GM062868 to V.S.P.; and National Research Service Award NIH-F30DK094541 to A.M.R.), the American Recovery and Reinvestment Act of 2009 (Public Law 111-5; MRI-R2 to V.S.P.), the Division of Intramural Research of the National Heart, Lung and Blood Institute (US National Institutes of Health; W.J.L., J.-X.L., P.L., S.M. and R.S.), the Stanford Medical Scientist Training Program (NIH-GM07365 to A.M.R.) and the Howard Hughes Medical Institute (K.C.G.).

AUTHOR CONTRIBUTIONS

A.M.R., D.F. and E.Ö. did crystallographic studies of the IL-15 quaternary complex; A.M.R. and E.Ö. determined and refined that structure; M.R. did SPR measurements; G.R.B. and V.S.P. did and analyzed molecular dynamics simulations; A.M.R. prepared cytokine proteins for signaling and transcriptional studies; A.M.R., S.M., I.M. and R.S. did signaling experiments by flow cytometry with phosphorylation-specific antibodies; A.M.R. did receptor-internalization studies; J.-X.L. and P.L. did and analyzed RNA sequencing transcriptional assays; J.-X.L. confirmed the quantitative PCR; A.M.R., J.-X.L., G.R.B., W.J.L. and K.C.G. designed the experiments; A.M.R., J.-X.L., P.L., S.M. and G.R.B. prepared the figures; A.M.R., W.J.L. and K.C.G. wrote the paper; and W.J.L. and K.C.G. supervised the research.

COMPETING FINANCIAL INTERESTS

The authors declare competing financial interests: details are available in the online version of the paper.

Published online at http://www.nature.com/doifinder/10.1038/ni.2449.
Reprints and permissions information is available online at http://www.nature.com/reprints/index.html.

1. Waldmann, T.A. The biology of interleukin-2 and interleukin-15: implications for cancer therapy and vaccine design. *Nat. Rev. Immunol.* **6**, 595–601 (2006).
2. Rochman, Y., Spolski, R. & Leonard, W.J. New insights into the regulation of T cells by gamma(c) family cytokines. *Nat. Rev. Immunol.* **9**, 480–490 (2009).
3. Sneller, M.C. *et al.* IL-15 administered by continuous infusion to rhesus macaques induces massive expansion of CD8+ T effector memory population in peripheral blood. *Blood* **118**, 6845–6848 (2011).
4. Liao, W., Lin, J.X. & Leonard, W.J. IL-2 family cytokines: new insights into the complex roles of IL-2 as a broad regulator of T helper cell differentiation. *Curr. Opin. Immunol.* **23**, 598–604 (2011).
5. Wuest, S.C. *et al.* A role for interleukin-2 trans-presentation in dendritic cell-mediated T cell activation in humans, as revealed by daclizumab therapy. *Nat. Med.* **17**, 604–609 (2011).
6. Stonier, S.W. & Schluns, K.S. Trans. -presentation: a novel mechanism regulating IL-15 delivery and responses. *Immunol. Lett.* **127**, 85–92 (2010).
7. Marks-Konczalik, J. *et al.* IL-2-induced activation-induced cell death is inhibited in IL-15 transgenic mice. *Proc. Natl. Acad. Sci. USA* **97**, 11445–11450 (2000).
8. Syed, R.S. *et al.* Efficiency of signalling through cytokine receptors depends critically on receptor orientation. *Nature* **395**, 511–516 (1998).
9. Wang, X., Rickert, M. & Garcia, K.C. Structure of the quaternary complex of interleukin-2 with its alpha, beta, and gammac receptors. *Science* **310**, 1159–1163 (2005).
10. Chirifu, M. *et al.* Crystal structure of the IL-15-IL-15Ralpha complex, a cytokine-receptor unit presented in trans. *Nat. Immunol.* **8**, 1001–1007 (2007).
11. Walter, T.S. *et al.* Lysine methylation as a routine rescue strategy for protein crystallization. *Structure* **14**, 1617–1622 (2006).
12. LaPorte, S.L. *et al.* Molecular and structural basis of cytokine receptor pleiotropy in the interleukin-4/13 system. *Cell* **132**, 259–272 (2008).
13. Collins, L. *et al.* Identification of specific residues of human interleukin 2 that affect binding to the 70-kDa subunit (p70) of the interleukin 2 receptor. *Proc. Natl. Acad. Sci. USA* **85**, 7709–7713 (1988).
14. Eisenman, J. *et al.* Interleukin-15 interactions with interleukin-15 receptor complexes: characterization and species specificity. *Cytokine* **20**, 121–129 (2002).

15. Pettit, D.K. *et al.* Structure-function studies of interleukin 15 using site-specific mutagenesis, polyethylene glycol conjugation, and homology modeling. *J. Biol. Chem.* **272**, 2312–2318 (1997).
16. Zurawski, S.M. *et al.* Definition and spatial location of mouse interleukin-2 residues that interact with its heterotrimeric receptor. *EMBO J.* **12**, 5113–5119 (1993).
17. Boulanger, M.J., Bankovich, A.J., Kortemme, T., Baker, D. & Garcia, K.C. Convergent mechanisms for recognition of divergent cytokines by the shared signaling receptor gp130. *Mol. Cell* **12**, 577–589 (2003).
18. McFarland, B.J. & Strong, R.K. Thermodynamic analysis of degenerate recognition by the NKG2D immunoreceptor: not induced fit but rigid adaptation. *Immunity* **19**, 803–812 (2003).
19. Dubois, S., Mariner, J., Waldmann, T.A. & Tagaya, Y. IL-15Ralpha recycles and presents IL-15 In trans to neighboring cells. *Immunity* **17**, 537–547 (2002).
20. Hanick, N.A. *et al.* Elucidation of the interleukin-15 binding site on its alpha receptor by NMR. *Biochemistry* **46**, 9453–9461 (2007).
21. Mortier, E. *et al.* Soluble interleukin-15 receptor alpha (IL-15R alpha)-sushi as a selective and potent agonist of IL-15 action through IL-15R beta/gamma. Hyperagonist IL-15 x IL-15R alpha fusion proteins. *J. Biol. Chem.* **281**, 1612–1619 (2006).
22. Rubinstein, M.P. *et al.* Converting IL-15 to a superagonist by binding to soluble IL-15R{alpha}. *Proc. Natl. Acad. Sci. USA* **103**, 9166–9171 (2006).
23. Rickert, M., Wang, X., Boulanger, M.J., Goriatcheva, N. & Garcia, K.C. The structure of interleukin-2 complexed with its alpha receptor. *Science* **308**, 1477–1480 (2005).
24. Levin, A.M. *et al.* Exploiting a natural conformational switch to engineer an interleukin-2 'superkine'. *Nature* **484**, 529–533 (2012).
25. Balasubramanian, S. *et al.* Ligand binding kinetics of IL-2 and IL-15 to heteromers formed by extracellular domains of the three IL-2 receptor subunits. *Int. Immunol.* **7**, 1839–1849 (1995).
26. Thanos, C.D., Randal, M. & Wells, J.A. Potent small-molecule binding to a dynamic hot spot on IL-2. *J. Am. Chem. Soc.* **125**, 15280–15281 (2003).
27. Bowman, G.R., Huang, X. & Pande, V.S. Using generalized ensemble simulations and Markov state models to identify conformational states. *Methods* **49**, 197–201 (2009).
28. Zambricki, E. *et al.* Signaling T-cell survival and death by IL-2 and IL-15. *Am. J. Transplant.* **5**, 2623–2631 (2005).
29. Castro, I., Yu, A., Dee, M.J. & Malek, T.R. The basis of distinctive IL-2- and IL-15-dependent signaling: weak CD122-dependent signaling favors CD8+ T central-memory cell survival but not T effector-memory cell development. *J. Immunol.* **187**, 5170–5182 (2011).
30. Cornish, G.H., Sinclair, L.V. & Cantrell, D.A. Differential regulation of T-cell growth by IL-2 and IL-15. *Blood* **108**, 600–608 (2006).
31. Lindemann, M.J., Hu, Z., Benczik, M., Liu, K.D. & Gaffen, S.L. Differential regulation of the IL-17 receptor by gammac cytokines: inhibitory signaling by the phosphatidylinositol 3-kinase pathway. *J. Biol. Chem.* **283**, 14100–14108 (2008).
32. Demirci, G. & Li, X.C. IL-2 and IL-15 exhibit opposing effects on Fas mediated apoptosis. *Cell Mol. Immunol.* **1**, 123–128 (2004).
33. Krieg, C., Letourneau, S., Pantaleo, G. & Boyman, O. Improved IL-2 immunotherapy by selective stimulation of IL-2 receptors on lymphocytes and endothelial cells. *Proc. Natl. Acad. Sci. USA* **107**, 11906–11911 (2010).
34. Ahmadzadeh, M. & Rosenberg, S.A. IL-2 administration increases CD4+ CD25(hi) Foxp3+ regulatory T cells in cancer patients. *Blood* **107**, 2409–2414 (2006).
35. Bessard, A., Sole, V., Bouchaud, G., Quemener, A. & Jacques, Y. High antitumor activity of RLI, an interleukin-15 (IL-15)-IL-15 receptor alpha fusion protein, in metastatic melanoma and colorectal cancer. *Mol. Cancer Ther.* **8**, 2736–2745 (2009).

## ONLINE METHODS

**Protein expression and purification.** For crystallization, the sequences encoding six-histidine-tagged human IL-15 (amino acids 1–114) in pET22b and six-histidine-tagged human IL-15Rα (amino acids 1–67) in pET26b were expressed together in the periplasm of BL21(DE3) *Escherichia coli* cells by induction for 20 h at 22 °C with isopropyl β-D-thiogalactopyranoside. The periplasmic fraction was isolated by osmotic shock and recombinant protein was purified by nickel–nitrilotriacetic acid chromatography followed by size-exclusion chromatography with a Superdex-75 column into HEPES-buffered saline (10 mM HEPES, pH 7.4, 150 mM NaCl and 0.02% sodium azide). Human IL-2Rβ (amino acids 1–214) with substitution of glutamine for asparagine at positions 3, 17 and 45 and human $\gamma_c$ (amino acids 34–232) with substitution of glutamine for asparagine at position 53 were expressed and purified from Hi5 insect cells as described[9]. Purified, *E. coli*–derived IL-15–IL-15Rα was then mixed with purified, insect-derived IL-2Rβ and $\gamma_c$ at a ratio of 1:1:1, followed by treatment with carboxypeptidases A and B overnight at 4 °C. The digested proteins were then methylated as described[11] and were purified by size-exclusion chromatography with a Superdex-200 column into HEPES-buffered saline.

For signaling and SPR experiments, IL-15 (amino acids 1–114) and IL-15 expressed together with IL-15Rα (amino acids 1–64) were produced in Hi5 cells and were purified by nickel–nitrilotriacetic acid and size-exclusion chromatography. Biotinylated IL-2Rβ was obtained by the addition of a carboxy-terminal biotin acceptor peptide tag (GLNDIFEAQKIEWHE) and coexpression with the addition of BirA ligase with excess biotin (100 μM) to the expression medium. Human IL-2 (1-133) and its high-affinity variant H9 were expressed and purified from Hi5 cells as described[24].

**Crystallization and data collection.** The purified, carboxypeptidase-treated and methylated IL-15–IL-15Rα–IL-2Rβ–$\gamma_c$ quaternary complex was concentrated to 12.1 mg/ml and crystallized by vapor diffusion in hanging-drops by addition of 0.1 μL crystallization solution (22.5% PEG3350, 0.1 M Bis-Tris propane, pH 8.75, and 0.2 M sodium acetate) to a volume of 0.1 μl protein. Crystals grew to a maximum size of 150 × 50 × 50 μm after 2–3 d at 22 °C. Crystals were cryoprotected in crystallization solution supplemented with 15% ethylene glycol and were flash-frozen in liquid nitrogen. A data set at 2.35Å was collected at beamline 8-2 at the Advanced Light Source and was processed with the HKL-3000 system for the integration of data reduction and structure solution[36].

**Structure determination and refinement.** The IL-15 quaternary complex structure was solved by molecular replacement with individual IL-2Rβ and $\gamma_c$ subunits from Protein Data Bank accession code 2B5I and the IL-15–IL-15Rα complex from Protein Data Bank accession code 2Z3Q. The Phenix software suite for the automated determination of macromolecular structures[37] was used for structural refinement and the COOT (Crystallographic Object-Oriented Toolkit) program for macromolecular model building, completion and confirmation[38] was used for model adjustment. Bulk solvent flattening was used for solvent correction. For the initial refinement, rigid body, coordinate and real-space refinement were used with individual atomic displacement parameter refinement. Translation, libration and screw-rotation refinement was added in later refinement iterations.

Buried surface area was calculated with the PISA server (protein interfaces, surfaces and assemblies)[39].

**Simulations and MSM.** The Gromacs 4.5.2 package[40] was used for molecular dynamics simulations with the Amber03 force field[41]. Each structure was placed in a dodecahedral box of about 6.6 × 6.6 × 4.7 nm and solvated with approximately 6,250 'transferable intermolecular potential, three-position model' water molecules. Conformations were first minimized with a steepest descent algorithm with a tolerance of 1,000 kJ/mol/nm and a step size of 0.01 nm. A cutoff of 1 nm was used for Coulombic and Van der Waals interactions and a grid-based neighbor list. Conformations were then equilibrated at 300K and 1 bar by holding protein atoms fixed and allowing the surrounding water to relax for 500 ps with a time step of 2 fs. All bonds were constrained with the LINCS algorithm[42]. Center-of-mass motion was removed at every step and a grid-based neighbor list with a cutoff of 1.5 nm was updated every 10 steps. For electrostatics, we used the fourth-order particle-mesh Ewald method[43] with a cutoff of 1.5 nm for Coulombic interactions, a Fourier spacing of 0.08 nm and a tolerance of $1^{-5}$. A hard cutoff of 1.2 nm was used for Van der Waals interactions with a switch starting at 1 nm. The temperature was controlled with the v-rescale thermostat[44] applied to both the protein and solvent with a time constant of 0.5 ps. The pressure was controlled with an isotropic Berenson barostat[45] applied to the entire system with a time constant of 0.5 ps and a compressibility of $4.5 \times 10^{-5}$ $bar^{-1}$. Long-range corrections were applied to energy and pressure. Production simulations up to 65 ns in length used the same parameters as for equilibration, with the exception that the protein atoms were no longer held fixed.

We used the MSMBuilder software package[27] to construct an MSM with a lag time of 1 ns. On the basis of published work on protein folding[46], we chose to create 208 clusters (microstates) with a hybrid k-centers–k-medoids algorithm and the r.m.s. deviation between pairs of conformations. All $C_\alpha$ and $C_\beta$ atoms were used for the r.m.s. deviation. Thermodynamic and kinetic properties were extracted from the eigenvalues and eigenvectors of MSM[47,48].

Assignment of residues to structural units used in r.m.s. deviation plots is provided in **Supplementary Table 1**; as with MSM, all $C_\alpha$ and $C_\beta$ atoms were used for these r.m.s. deviations.

**SPR.** A Biacore T100 was used for SPR at 25 °C. Protein concentrations were quantified by ultraviolet spectroscopy at 280 nm with a Nanodrop2000 spectrometer (Thermo Scientific). Experiments were done on a Biacore SA sensor chip (GE Healthcare), which was used to capture biotinylated IL-2Rβ ($R_{max}$ ~80 RU). To control for nonspecific binding, an unrelated biotinylated protein was immobilized with an RU value matching that of the reference surface. Measurements were made with serial dilutions of IL-15 or IL-15–IL-15Rα in HBS-P+ buffer (GE Healthcare) diluted to a concentration of 1× and supplemented with 0.01% BSA. The IL-2Rβ surface was regenerated with 10 mM sodium acetate (pH 5.5) and 1 M $MgCl_2$. All data were analyzed with the Biacore T100 evaluation software version 2.0 with a 1:1 Langmuir binding model.

**Mice.** Animal protocols were approved by the Animal Care and Use Committee of the National Heart, Lung, and Blood Institute and followed the US National Institutes of Health Guideline "Using Animals in Intramural Research."

**Cell lines.** YT-1 cells were maintained in complete RPMI-1640 medium (Gibco) in a humidified incubator at 37 °C and 5% $CO_2$. IL-2Rα$^+$ YT-1 cells were obtained by enrichment with by magnetic sorting with phycoerythrin-conjugated anti-IL-2Rα (BC96; Biolegend) and paramagnetic microbeads coated with anti-phycoerythrin (Miltenyi Biotec). Enrichment for IL-2Rα$^+$ cells was assessed by flow cytometry in the FL2 channel with an Accuri C6 flow cytometer.

**Analysis of intracellular signaling via STAT5 and Erk1-2 by flow cytometry with phosphorylation-specific antibodies.** For dose-response experiments, serial dilutions of IL-15, IL-15–IL-15Rα, IL-2 or H9 were applied to IL-2Rα$^-$ or IL-2Rα$^+$ YT-1 cells in a 96-well plate ($2 \times 10^5$ cells per well). After 10 min, cells were fixed in paraformaldehyde and permeabilized in 100% methanol. For analysis of signaling kinetics, 1 or 500 nM μM IL-15–IL-15Rα, IL-2 or H9 was applied to YT-1 cells ($2 \times 10^5$ cells per well) and cells were fixed after 1, 2.5, 5, 15, 30, 60 or 120 min) and were permeabilized with 100% methanol. Samples in methanol were 'multiplexed' (that is, many samples were combined into one tube before staining) through the use of 'fluorescent barcoding' (a means by which each sample is labeled with a different signature)[49] with amine-reactive DyLight 800 dye (Thermo Scientific) and Pacific blue dye (Invitrogen), then were stained with Alexa Fluor 647–conjugated anti-STAT5 pY694 (562076; BD Biosciences) and Alexa Fluor 488–conjugated anti-Erk1-2 pT202/pY204 (4344S; Cell Signaling Technology). Mean cell fluorescence was determined with an LSR II (BD). Dose-response and kinetic curves and $EC_{50}$ values were calculated with GraphPad Prism.

**Isolation of CD8$^+$ cells and analysis of intracellular signaling via STAT5 and S6 by flow cytometry with phosphorylation-specific antibodies.** Mouse CD8$^+$ T cells were isolated from spleens and lymph nodes of C57BL/6 mice by negative enrichment for CD8$^+$ T cells (CD8a$^+$ T cell Isolation kit II; Miltenyi Biotec). For cytokine-stimulation assays with freshly isolated cells, cells were





doi:10.1038/ni.2449

used immediately. For the generation of *in vitro* preactivated $CD8^+$ T cells, six-well plates were precoated with 2 μg/ml of plate-bound monoclonal anti-CD3 (2C11; produced in-house). $CD8^+$ cells were seeded at a density of $1 \times 10^6$ cells per ml with 1 μg/ml of soluble monoclonal anti-CD28 (37.51; BD). Cells were cultured for 2 d with stimulation of the T cell antigen receptor, followed by 6 h of rest in fresh culture medium.

For signaling-kinetics experiments with freshly isolated $CD8^+$ T cells, 1 or 500 nM of IL-15, IL-15–IL-15Rα, IL-2 or H9 was applied to $2 \times 10^5$ $CD8^+$ T cells per well. For signaling-kinetics experiments with preactivated $CD8^+$ T cells, 10 pM or 10 nM of IL-15, IL-15–IL-15Rα, IL-2 or H9 was used for stimulation. $CD8^+$ T cells were fixed immediately after cytokine stimulation with PhosFlow Lyse/Fix buffer (BD) and then were permeabilized with PhosFlow Perm Buffer III (BD). Cells were then stained at room temperature for 30 min in the dark with phycoerythrin-conjugated antibody to STAT5 phosphorylated at Tyr694 (562077; BD Biosciences) and Alexa Fluor 647–conjugated antibody to S6R phosphorylated at Ser235 and Ser236 (D57.2.2E; Cell Signaling Technology). Data were acquired on a FACSCanto (BD Biosciences) and analyzed with FlowJo (Tree Star).

**Receptor-internalization experiments.** IL-15, IL-15–IL-15Rα, IL-2 or H9 (500 nM) was applied to $2 \times 10^5$ YT-1 cells in a 96-well plate for 1, 2.5, 5, 15, 30, 60 or 90 min, after which cells were immediately transferred to ice to prevent further receptor internalization. Cells were washed twice with ice-cold FACS buffer (0.5% BSA and 0.5 mM EDTA in PBS) and then were stained for 30 min on ice with allophycocyanin-conjugated anti-human IL-2Rβ (TUGh4; Biolegend) diluted 1:50. Cells were washed twice more with ice-cold FACS buffer and then were fixed for 10 min at room temperature with 1.5% paraformaldehyde in PBS. After fixation, mean cell fluorescence was determined with an Accuri C6 flow cytometer.

**RNA sequencing.** Splenic $CD8^+$ T cells were isolated from 6-week-old female C57BL/6 mice and treated with 1 nM or 500 nM of IL-2 or IL-15 for the appropriate time, and total RNA was isolated. Three samples treated identically were pooled, then cDNA was synthesized with 2.5 ng of the pooled RNA and amplified by a two-step PCR process (twelve cycles with UP1 and UP2 primers (**Supplementary Table 2**) followed by nine cycles with AUP1* and AUP2* primers (**Supplementary Table 2**) as described)[50]. After fragmentation with a Bioraptor (Diagenode), fragments 220–400 base pairs in length were isolated with 2% E-Gel (Invitrogen), then ends were repaired and adaptor (Illumina) was added with T4 DNA ligase (New England Biolabs), followed by amplification for seventeen cycles with PE 1.0 and PE 2.0 primers (Illumina) and Phusion High Fidelity PCR Master Mix (New England Biolabs). PCR products were 'barcoded' (indexed) and sequenced on an Illumina HiSeq 2000 platform.

**RNA sequencing data analysis.** Sequenced reads (single-end 36 base pairs) were aligned to the RefSeq mouse gene database (mm8 revision) with the ELAND pipeline. Raw reads that fell on exons of each gene were counted and normalized reads per kilobase of exon model per million mapped reads were calculated for each gene. The statistical packages in software of the R project for statistical computing were used for multidimensional scaling, linear-regression modeling and analysis of differences in gene expression.

**Gene-expression analysis by real-time RT-PCR.** First, cDNA was synthesized with 200 ng total RNA, oligo(dT) and Ominscript RT kit (Qiagen), then RT-PCR was done with an ABI 7900 HD Sequence Detection System (primers, (**Supplementary Table 2**) and TaqMan 2× PCR Master mix (ABI/Ambion). Relative expression was calculated based on the cycle number for the control gene *Rpl7*, as its expression was constant under the experimental conditions.


36. Minor, W., Cymborowski, M., Otwinowski, Z. & Chruszcz, M. HKL-3000: the integration of data reduction and structure solution–from diffraction images to an initial model in minutes. *Acta Crystallogr. D Biol. Crystallogr.* **62**, 859–866 (2006).
37. Adams, P.D. *et al.* PHENIX: building new software for automated crystallographic structure determination. *Acta Crystallogr. D Biol. Crystallogr.* **58**, 1948–1954 (2002).
38. Emsley, P. & Cowtan, K. Coot: model-building tools for molecular graphics. *Acta Crystallogr. D Biol. Crystallogr.* **60**, 2126–2132 (2004).
39. Krissinel, E. & Henrick, K. Inference of macromolecular assemblies from crystalline state. *J. Mol. Biol.* **372**, 774–797 (2007).
40. Hess, B., Kutzner, C., van der Spoel, D. & Lindahl, E. GROMACS 4: Algorithms for highly efficient, load-balanced, and scalable molecular simulation. *J. Chem. Theory Comput.* **4**, 435–447 (2008).
41. Duan, Y. *et al.* A point-charge force field for molecular mechanics simulations of proteins based on condensed-phase quantum mechanical calculations. *J. Comput. Chem.* **24**, 1999–2012 (2003).
42. Hess, B. P-LINCS: A parallel linear constraint solver for molecular simulation. *J. Chem. Theory Comput.* **4**, 116–122 (2008).
43. Darden, T., York, D. & Pedersen, L. A smooth particle mesh Ewald potential. *J. Chem. Phys.* **103**, 3014–3021 (1995).
44. Bussi, G., Donadio, D. & Parrinello, M. Canonical sampling through velocity rescaling. *J. Chem. Phys.* **126**, 014101 (2007).
45. Berendsen, H.J.C., Postma, P.M., van Gunsteren, W.F., DiNola, A. & Haak, J.R. Molecular dynamics with coupling to an external bath. *J. Chem. Phys.* **81**, 3684–3690 (1984).
46. Bowman, G.R., Beauchamp, K.A., Boxer, G. & Pande, V.S. Progress and challenges in the automated construction of Markov state models for full protein systems. *J. Chem. Phys.* **131**, 124101 (2009).
47. Bowman, G.R., Huang, X. & Pande, V.S. Network models for molecular kinetics and their initial applications to human health. *Cell Res.* **20**, 622–630 (2010).
48. Noe, F. & Fischer, S. Transition networks for modeling the kinetics of conformational change in macromolecules. *Curr. Opin. Struct. Biol.* **18**, 154–162 (2008).
49. Krutzik, P.O. & Nolan, G.P. Fluorescent cell barcoding in flow cytometry allows high-throughput drug screening and signaling profiling. *Nat. Methods* **3**, 361–368 (2006).
50. Tang, F. *et al.* RNA-Seq analysis to capture the transcriptome landscape of a single cell. *Nat. Protoc.* **5**, 516–535 (2010).